Temporal stability and correctability of a MWIR T2SL focal plane array

I. Ribet-Mohamed, J. Nghiem, M. Caes, M. Guenin, L. Höglund, E. Costard, J.B. Rodriguez, Philippe Christol

Temporal stability and correctability of a MWIR T2SL focal plane array

I. Ribet-Mohamed[1], J. Nghiem[1], M. Caes[1], M. Guénin[1], L. Höglund[2], E. Costard[2], J.B. Rodriguez[3], P. Christol[3]
[1] ONERA, Chemin de la Hunière, F- 91761 Palaiseau, France.
[2]IRnova AB, Electrum 236, SE-164 40 Kista, Sweden
[3]IES, Univ. Montpellier, CNRS, F-34000 Montpellier, France

Abstract

Stability over time has recently become a figure of merit of major importance to compare the performances of infrared focal plane arrays (FPA) of different technologies. Indeed, this parameter dictates how often the calibration of operational electro-optical systems has to be done, and thus reflects the availability of the system during an operational mission. Recent studies also showed that random telegraph signal (RTS) noise, which leads to flickering pixels, can strongly affect the image quality.

The stability over time is generally estimated through fixed pattern noise (FPN) and residual fixed pattern noise (RFPN) measurements after a two-point correction. However, each laboratory or industrial has its own protocols and criteria, such that published results cannot be easily compared.

In this paper, we describe our experimental protocol to evaluate the stability over time of a FPA and to count up / classify flickering pixels. We then present the results of two measurement campaigns realized on a T2SL MWIR Integrated Detector Dewar Cooler Assembly (IDDCA) provided by IRnova: the first, long term study was dedicated to the measurement of FPN/RFPN (estimated with two different algorithms); with the second study, dedicated to RTS noise, we tried to realize a classification of flickering pixels, based on the jump amplitude and the jump frequency. Our measurements show that the stability over time and correctability of the T2SL MWIR IDDCA are excellent.

Highlights :
- Stability over time and RTS noise of a commercial T2SL midwave infrared FPA have been investigated.
- RFPN/TN ratio stays lower than unity for more than 7 weeks
- number of RTS pixels is as low as 10 for a 5-minutes long measurement

Keywords: stability over time, FPN, RFPN, correctability, T2SL, MWIR, FPA

[*]Corresponding author: Tel.: (+33) 180 386 362; e-mail address: isabelle.ribet@onera.fr

Introduction

Type-II Superlattice (T2SL) is a recent infrared detection technology whose excellent electro-optical performances (expressed as quantum efficiency, dark current density, specific detectivity or NETD) have been widely reported from the shortwave to the very longwave infrared domains [1-10]. They thus position themselves in competition with well-established cooled infrared technologies (HgCdTe, InSb, XBn, QWIP, etc) for high-performance applications such as radiometric imaging. Therefore, more system-oriented merit functions deserve to be evaluated, such as MTF [11] (Modulation Transfer Function, which describes how well a detector can reproduce spatial frequencies). Studying the stability over time is also of great interest, since it dictates how often the calibration of operational electro-optical systems has to be done, and thus reflects the availability of the system during an operational mission.

The stability over time is generally estimated through fixed pattern noise (FPN) and residual fixed pattern noise (RFPN) measurements, the latter being evaluated after a linear two-point calibration (TPC). However, each laboratory or industrial has its own protocol and criteria to exclude some pixels considered as defective, such that published results cannot be easily compared. Moreover, FPN and RFPN don't necessarily detect pixels with random telegraph signal (RTS) noise. The signal delivered by these pixels can oscillate between two (or more) levels at certain times, creating a particularly harmful blinking effect for image quality. Since the blinking is not permanent, detecting these pixels is a very difficult task.

In this paper, we describe our experimental protocol to evaluate the temporal stability of a FPA. We then present the results of long-term measurement campaigns realized on an InAs/GaSb T2SL focal plane array. We chose to carry out our measurements on a detector integrated in an operational packaging (IDDCA, which means Integrated Detector Dewar Cooler Assembly) in order to remain as close as possible to the real conditions of use. More precisely, our measurements were realized on a T2SL MWIR 320x256 pixels IDDCA provided by IRnova, on which we have already published very encouraging first stability over time measurements [12].

The first paragraph of this paper is dedicated to residual fixed pattern noise (RFPN) measurements. After recalling the principle of this measurement, we present our experimental setup and the data processing. Results obtained during a long-term measurement campaign are then reported and commented. The second paragraph focuses on random telegraph signal (RTS) noise, and presents the experimental setup, the data processing and the experimental results.

Residual fixed pattern noise measurements

The stability over time is generally estimated through fixed pattern noise (FPN). The FPN corresponds to the spatial fluctuations of the signal delivered by the pixels of a focal plane array (FPA) when it receives a homogeneous incident power. The fixed pattern noise can originate in the pixel itself (for example if there are differences in cut-off wavelengths or

variations in active area thickness through the focal plane array) or in the read-out integrated circuit (for example if the output amplifiers have slightly different characteristics (gain, offset)). Non-uniformity correction (NUC) is generally realized with a linear two-point calibration [13]. To implement it, two uniform backgrounds are presented to the FPA (generated for example with two extended blackbodies at different temperatures). Assuming that the signal delivered by each pixel varies linearly with the incident power, one can calculate, for each pixel, a gain correction coefficient $G_{i,j}$ and an offset correction coefficient $O_{i,j}$, accounting for multiplicative and additive non-uniformities, respectively. They are defined as :

$$G_{i,j} = \frac{S_{i,j}(\phi_1) - S_{i,j}(\phi_2)}{\langle S_{i,j}(\phi_1)\rangle - \langle S_{i,j}(\phi_2)\rangle} \quad (1)$$

$$O_{i,j} = S_{i,j}(\phi_1) - G_{i,j} \cdot \langle S_{i,j}(\phi_1)\rangle \quad (2)$$

where $S_{i,j}(\phi_1)$ (resp. $S_{i,j}(\phi_2)$) is the signal delivered by the pixel (i,j) for an incident power equal to ϕ_1 (resp. ϕ_2) and after removing the ROIC offset ; $<S_{i,j}(\phi_1)>$ (resp. $<S_{i,j}(\phi_2)>$) is the spatially averaged signal delivered by the FPA (after removing the ROIC offset) for an incident power equal to ϕ_1 (resp. ϕ_2).

After 2 points correction, the signal delivered by the pixel (i,j) becomes:

$$S'_{i,j}(\phi) = \frac{S_{i,j}(\phi) - O_{i,j}}{G_{i,j}} \quad (3)$$

When applying the two-point correction that has just been calculated, the corrected image is perfectly uniform at an incident power equal to ϕ_1 or ϕ_2.

The two-point calibration has the advantage of being easy to implement and very effective at the time it is calculated. But the question is how long this calibration remains valid. To answer this question, the fixed spatial noise that remains after the two-point correction - called residual fixed spatial noise (RFPN) - is evaluated:

$$RFPN(\phi) = \sqrt{\frac{1}{N} \cdot \sum_i \sum_j \left(S_{i,j}(\phi) - \langle S_{i,j}(\phi)\rangle\right)^2} \quad (4)$$

where N is the total number of pixels of the FPA.

To evaluate the performance of a system, temporal noise and residual fixed pattern noise are generally summed quadratically[14], the former being defined as the temporal fluctuations of the signal delivered by a pixel. Consequently, the influence of spatial noise decreases rapidly as soon as the RFPN is lower than the temporal noise; therefore, one can consider that the calibration is valid as long as the RFPN remains lower than the temporal noise, even if stricter criteria have been proposed for particular conditions [15] (with a human observer in the loop).

Experimental setup

The measuring bench relies on an extended area blackbody which is placed in front of the IDDCA. Scanning the blackbody temperature allows to scan the incident power on the focal plane array. For each blackbody temperature explored, a 256-image cube is recorded at an integration time of 4ms, and another one at null integration time to measure the read-out integrated circuit (ROIC) offset.

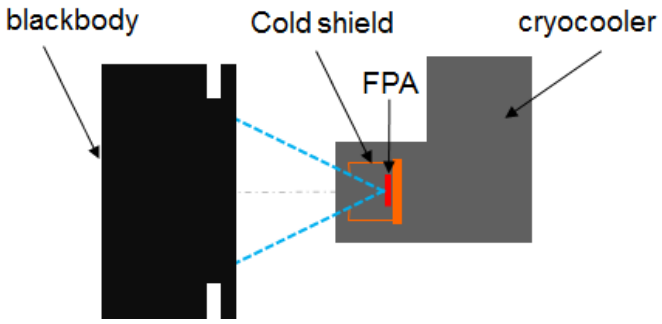

Figure 1 – Experimental setup for the stability over time measurements.

Data processing

The analysis of the measurements consists of three main stages:

- the detection of defective pixels, and once these have been set aside,
- the application of the two-point correction
- the calculation of the residual fixed pattern noise

In order to highlight the importance of the criteria used to define a defective pixel, we compared several algorithms. The first one, which will be further referred as the reference algorithm, considers the average image recorded for a 50% well fill and corrects it for the dome effect due to variation in the geometrical throughput between the center and the corner of the focal plane array. It then sets aside pixels with continuous level, noise (defined as the standard deviation of the signal of one pixel over 256 images), responsivity or noise equivalent temperature difference (NETD) too far from the average values. The exact criteria are summarized in Table 1, together with the number of pixels falling into each category. The total number of defective pixels detected with this algorithm is 41, which corresponds to an operability of 99.95%. As can be seen in Figure 2, the spatial distribution of the defective pixels is relatively homogeneous, with only 3 clusters with 2x1 pixels, and no bigger cluster.

	Criteria	Number of pixels
Continuous level	$\left\|S_{i,j} - \langle S_{i,j} \rangle\right\| > 30\% \cdot \langle S_{i,j} \rangle$	31
Noise	$\left\|\sigma_{i,j} - \langle \sigma_{i,j} \rangle\right\| > 50\% \cdot \langle \sigma_{i,j} \rangle$	25
Responsivity	$\left\|R_{i,j} - \langle R_{i,j} \rangle\right\| > 30\% \cdot \langle R_{i,j} \rangle$	34
NETD	$\left\|NETD_{i,j} - \langle NETD_{i,j} \rangle\right\| > 100\% \cdot \langle NETD_{i,j} \rangle$	37
Total		41

Table 1 – Criteria used to classify one pixel as a defective one (reference algorithm). $S_{i,j}$ is the signal delivered by the pixel, $< S_{i,j} >$ is the spatially averaged signal, $\sigma_{i,j}$ is the noise of the pixel, $<\sigma_{i,j}>$ is the spatially averaged noise, $R_{i,j}$ is the

responsivity of the pixel, $< R_{i,j} >$ is the spatially averaged responsivity, $NETD_{i,j}$ is the NETD of the pixel and $<NETD_{i,j}>$ the spatially averaged NETD. The total number of defective pixels is lower than the sum of the number of pixels sorted as defective with only one criterion, since most of the defective pixels fall into more than one category.

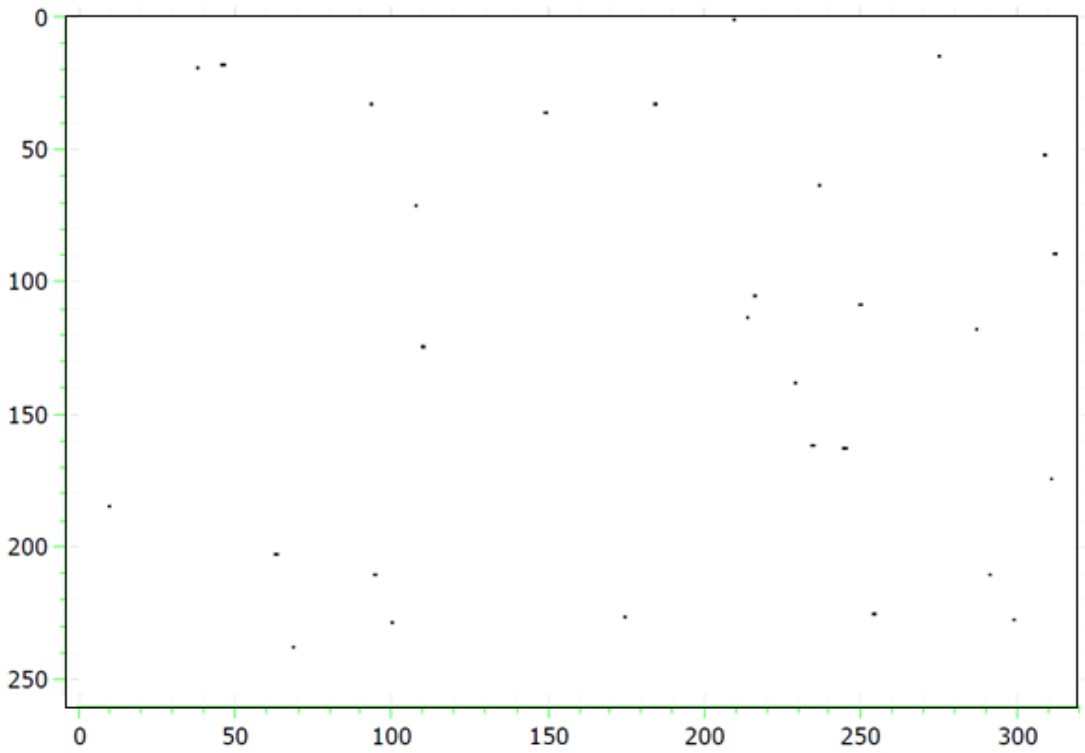

Figure 2 – Defective pixels map detected with the reference algorithm. 41 pixels are set aside, which represents an operability of 99.95%.

The second algorithm, which we will call advanced algorithm, is based on the same principle, except that a two-point correction (calculated from images at 33% and 66% well fill) is applied after the dome effect is corrected and before the defective pixels are detected. The exact criteria are summarized in Table 2, together with the number of pixels falling into each category. The total number of defective pixels detected with this algorithm is 49, which corresponds to an operability of 99.94%. As can be seen on the defective pixels map presented in Figure 3, the spatial repartition of defective pixels is once again quite homogeneous.

	Criteria	Number of pixels
Continuous level	$\left\|S_{i,j} - \left\langle S_{i,j} \right\rangle\right\| > 10 \cdot \left\langle \sigma_{i,j} \right\rangle$	43
Noise	$\left\|\sigma_{i,j} - \left\langle \sigma_{i,j} \right\rangle\right\| > 50\% \cdot \left\langle \sigma_{i,j} \right\rangle$	25
Responsivity	$\left\|R_{i,j} - \left\langle R_{i,j} \right\rangle\right\| > 30\% \cdot \left\langle R_{i,j} \right\rangle$	34
NETD	$\left\|NETD_{i,j} - \left\langle NETD_{i,j} \right\rangle\right\| > 100\% \cdot \left\langle NETD_{i,j} \right\rangle$	37
Total		49

Table 2 – Criteria used to classify one pixel as a defective one (advanced algorithm).

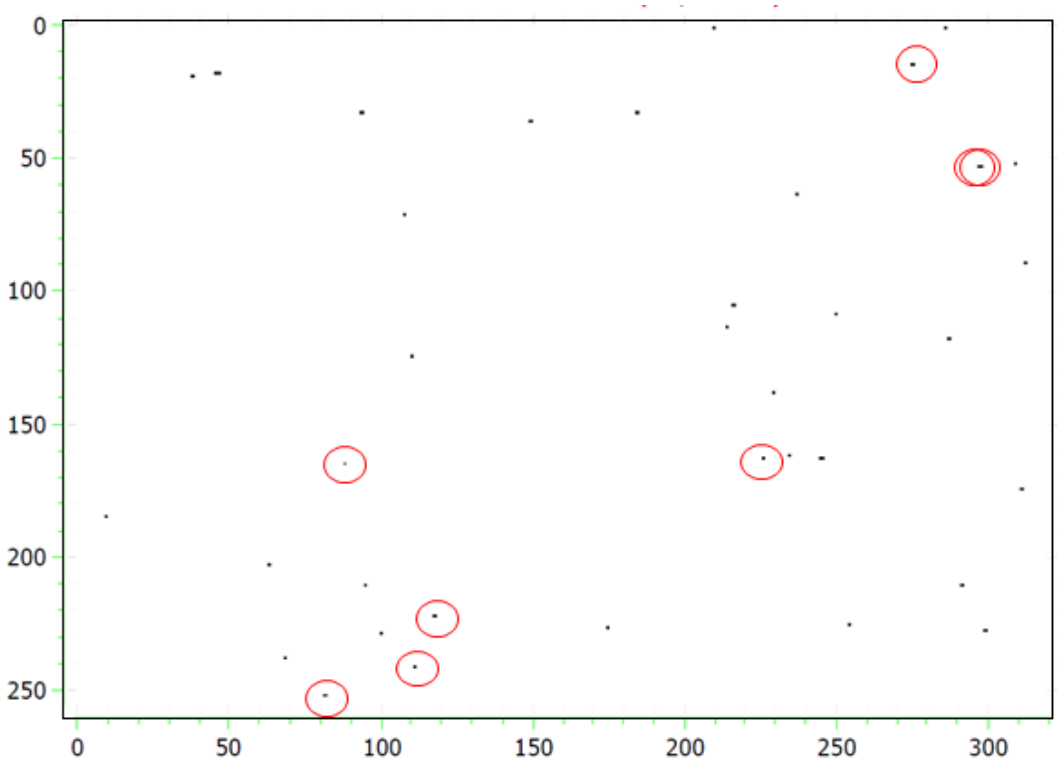

Figure 3 - Defective pixels map detected with the advanced algorithm. 49 pixels are set aside, which represents an operability of 99.94%. The 8 pixels which were not detected by the reference algorithm (Figure 2) are highlighted by red circles.

Once the defective pixels have been set aside, we apply the gain and offset corrections (see equation (3)) and then calculate the residual fixed pattern noise thanks to equation (4). Results are presented in the following paragraph.

Results and discussion

Figure 4 presents the ratio between the residual fixed pattern noise and the temporal noise (TN) as a function of the well fill factor. The left-hand side (resp. right-hand side) graph corresponds to the case where defective pixels are detected with the reference algorithm (resp. advanced algorithm). In both cases, the gain and offset corrections were calculated on the first day of the campaign. The RFPN/TN results obtained that day exhibit the expected W-shape, reaching zero for the two values of the power used to calculate the gain and offset coefficients. The RFPN/TN measurements obtained on the following days are all higher than those obtained on the first day, but if we trace their temporal evolution (see Figure 5), it appears that the RFPN is remarkably stable over 6 weeks. More precisely, the ratio between the RFPN and the temporal noise is typically equal to 1.1 for the reference algorithm and equal to 0.83 for the advanced algorithm.

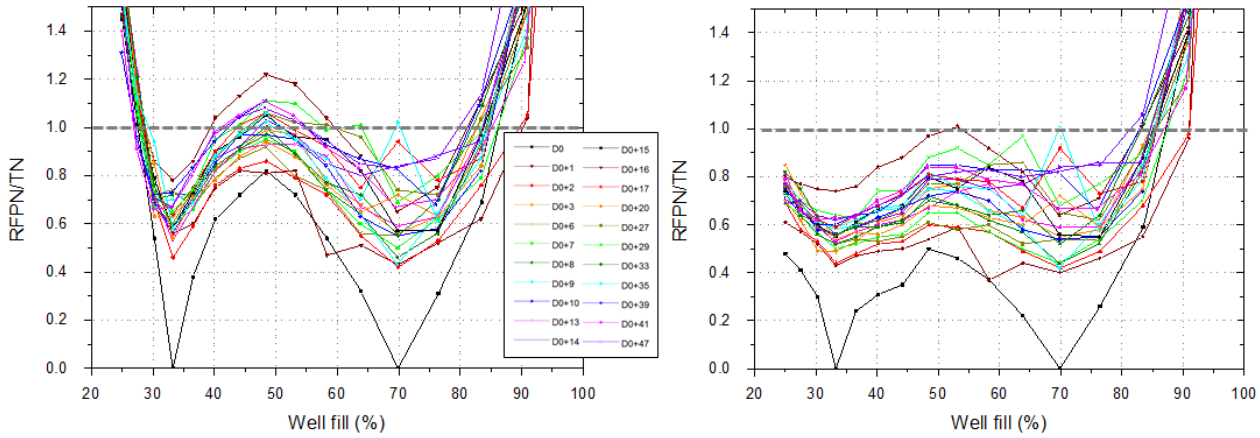

Figure 4 - Ratio between residual fixed pattern noise (RFPN) and temporal noise (TN) as a function of well fill, for measurements realized during 7 weeks. Left : 41 defective pixels (identified with the reference algorithm) were set aside ; Right : 49 defective pixels (identified with the improved algorithm) were set aside. The gain and offset coefficient used in the two-point corrections are those calculated on the first day of the campaign.

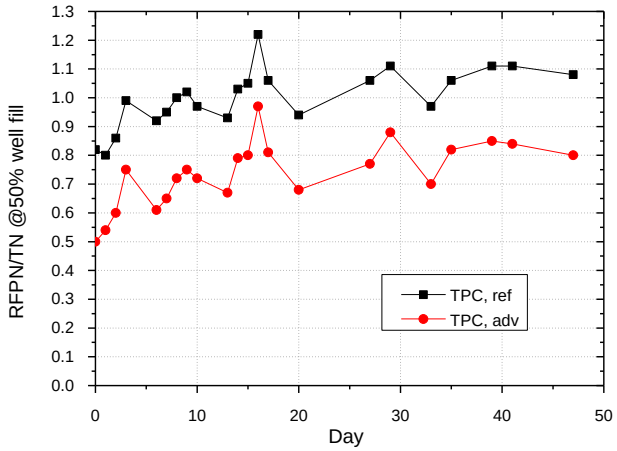

Figure 5 – Temporal evolution of the ratio between the residual fixed pattern noise and the temporal noise at 50% well fill, using the reference algorithm or the advanced one to detect defective pixels. The gain and offset coefficient used in the two-point corrections are those calculated on the first day of the campaign.

These first results clearly show that the temporal stability of the T2SL MWIR FPA is excellent. They also stress the importance of the data processing phase and the criteria used to rule out defective pixels, since removing 8 more pixels decreases the RFPN/TN plateau of 25%. It appeared that these 8 pixels presented a signal close to the average for 50% well fill (and were therefore not detected with the reference algorithm), but that they were strongly non-linear and impossible to correct with a TPC calibration. That's why the second algorithm detected them.

Up to now, we calculated the gain and offset coefficients using the image cubes recorded the first day of the campaign. But some electro-optical systems integrate a shutter that regularly records an updated average image at a given temperature (that of the shutter), sometimes used to perform a 1-point correction during instrument use.

To go further in our analysis, we now propose to use a two-point correction where one of the image cubes dates back to the first day of the campaign and the second one is updated and corresponds to the actual operating conditions. Figure 6 presents the results obtained for an update of the low temperature image cube (33% well fill) and for an update of the high temperature image cube (66% well fill). Refreshing one of the image cubes maintains the quality of the correction at the corresponding incident power. The effect on the temporal evolution of the RFPN/TN ratio is visible in Figure 7, with a plateau decreasing to 0.6 with an update of the low blackbody temperature image cube, and reaching 0.5 with an update of the high blackbody temperature image cube. This is two times lower than the value obtained with the basic data processing (also reported on this graph for the sake of comparison). Moreover, if we fit these measurements and extrapolate them we find a period of validity of this new two-point correction (defined as the moment when the RFPN/TN reaches 1) higher than 180 days, to be compared to 18 days for the basic TPC with reference defective pixels detection algorithm, and 70 days for the basic TPC with advances defective pixels detection algorithm.

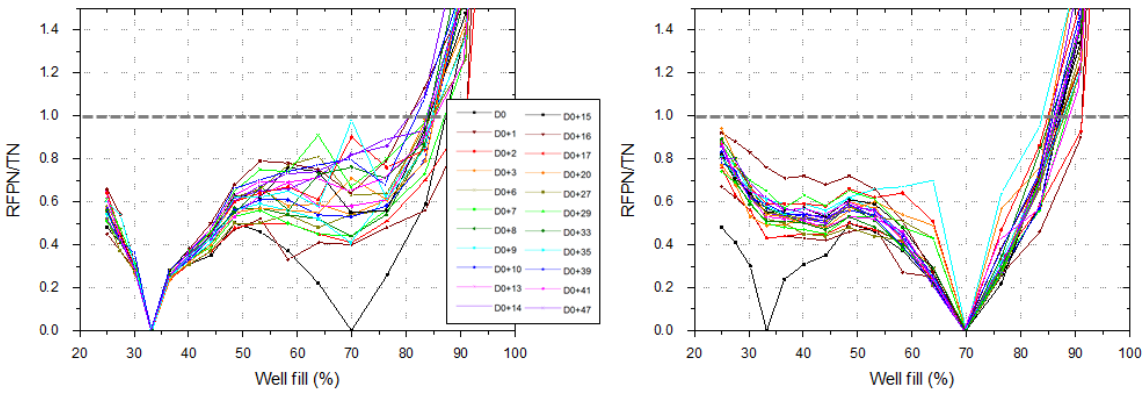

Figure 6 - Ratio between residual fixed pattern noise and temporal noise as a function of well fill, for measurements realized during 7 weeks. The two-point correction uses one image cube recorded on the first day of the campaign, and the other one updated on the day of the measurement. Left : low-temperature update (corresponding to a WF=33%) ; Right : high-temperature update (corresponding to a WF=66%).

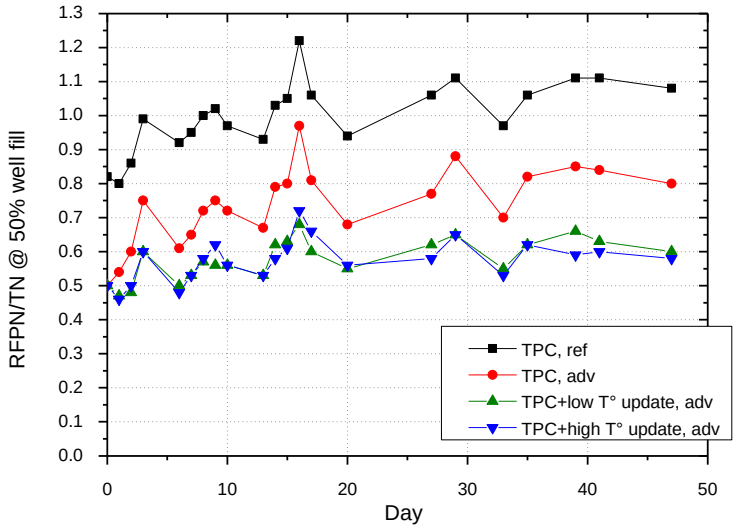

Figure 7 - Temporal evolution of the ratio between the residual fixed pattern noise and the temporal noise @ 50% well fill, obtained with different data processing algorithms. Black curve : reference algorithm to detect defective pixels and two-point correction (TPC) with gain and offset coefficients calculated on the first day of the campaign ; Red curve : advanced algorithm to detect defective pixels and TPC with gain and offset coefficients calculated on the first day of the campaign ; Green and blue curves : advanced algorithm to detect defective pixels and TPC with low temperature image and high temperature image upgrade, respectively.

To finish with, we decided to test the effectiveness of the 2-point correction in the long term. For this purpose, we applied the 2-point correction determined in 2015 on images acquired in 2018,, see Figure 8. As expected, the RFPN/TN ratio is higher than one, but is lower than two, to be compared with a FPN/TN ratio (before 2-point correction) of 35. This is coherent with the excellent temporal stability measured before.

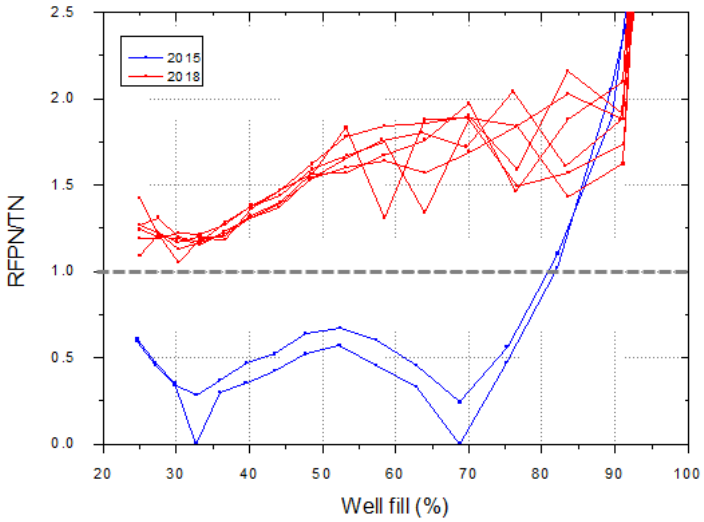

Figure 8 - Ratio between residual fixed pattern noise (RFPN) and temporal noise (TN) as a function of well fill, for measurements realized in 2015 (blue) and 2018 (red). The gain and offset coefficient used in the two-point corrections are those calculated in 2015. 48 pixels were set aside by the advanced defective pixels detection algorithm.

Random telegraph signal noise study

Pixels are considered as exhibiting random telegraph signal (RTS) noise when their signal oscillates between at least two levels, while the received power and operating conditions do not change. RTS noise can be particularly detrimental to image quality since the resulting blinking effect cannot be suppressed by 2-point correction. It is thus considered as a major challenge that different technologies will have to face [16-18], especially in addressing high operating (HOT) and size, weight and power (SWaP) requirements.

Experimental setup and data processing

To study RTS noise, we used the same test bench as before, setting the blackbody temperature at 30°C and the integration time at 4ms. We recorded 17 cubes of 1024 images, which represents nearly 5 minutes of cumulative acquisition. Some of the measurements were made within the same cooling, others after allowing the detector to return to room temperature.

To detect RTS pixels, we developed an algorithm which starts by isolating those with excess temporal noise. Among these candidates, it then fits the histogram with one or several Gaussian functions: if two or more Gaussian functions are required, the pixel is considered as affected by RTS noise (see example Figure 9). The levels are extracted from the maxima of the Gaussian functions, and the average time spent on each level is also calculated.

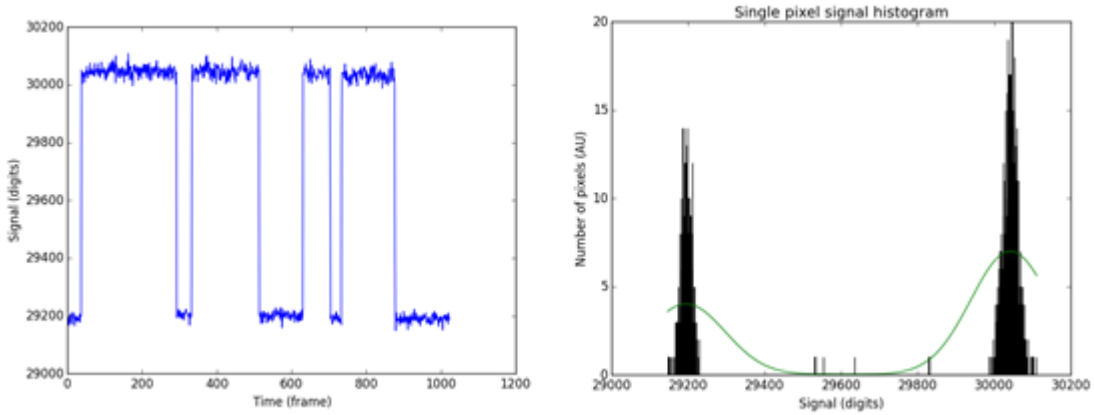

Figure 9 – Left : signal delivered by a pixel affected by a 2-level RTS noise as a function of time ; Right : associated histogram, showing two distinct populations.

Results and discussion

Our measurements show that the number of RTS pixels of this 320x256 pixels FPA is very low. It varies between 1 and 5 pixels detected by acquisition of 1024 images (with a mean value of 2 RTS pixel per cube). Table 3 presents a classification of the 10 blinking pixels detected on all acquisitions (17 cubes). Only 4 pixels have a true 2-level behaviour, 2 pixels exhibit spikes, 1 pixel exhibits a complicated behaviour that could be interpreted in terms of spikes + 2-level, and 3 pixels only present excess noise.

Category	Pixels list	Occurrence (% of acquired cubes)	Total number of pixels in each category
2-level	5409 10309 37780 66005	88% 6% 12% 6%	4
Spikes	22950 33291	18% 18%	2
2-level + spikes	40610	18%	1
Excess noise	1059 10310 36705		3
Total number of RTS pixels detected			10

Table 3 – Classification of pixels detected as affected by RTS noise.

We also plotted in Figure 10 the cumulative number of RTS pixels detected as a function of the measurement number. This number increases, but the evolution seems not dictated by changes in cooling cycles (materialized by arrows).

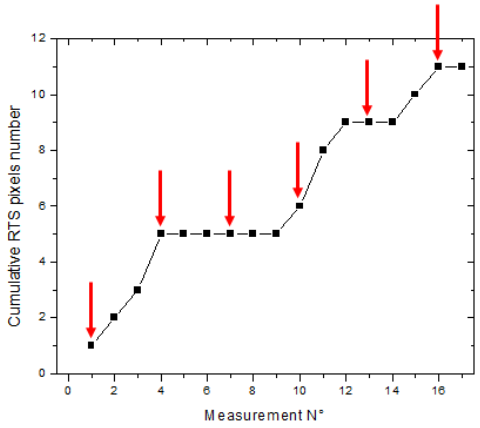

Figure 10 – Cumulative number of RTS pixels detected as a function of the measurement number. Red arrows indicate new cooling cycles.

Pixels jumping between two different states can be classified according to features such as the jump amplitude and the up and down mean times [17]. The only 2-level pixel with enough jumps to conduct such analysis is pixel n°5409 (see Figure 11). We find a jump amplitude of 858 digits (i.e. 65.4mV), and up and down mean times of 210ms (standard deviation : 200 ms) and 105ms (standard deviation : 100 ms), respectively. In order to confirm these values and go further into our analysis, new measurements on a longer time scale are required.

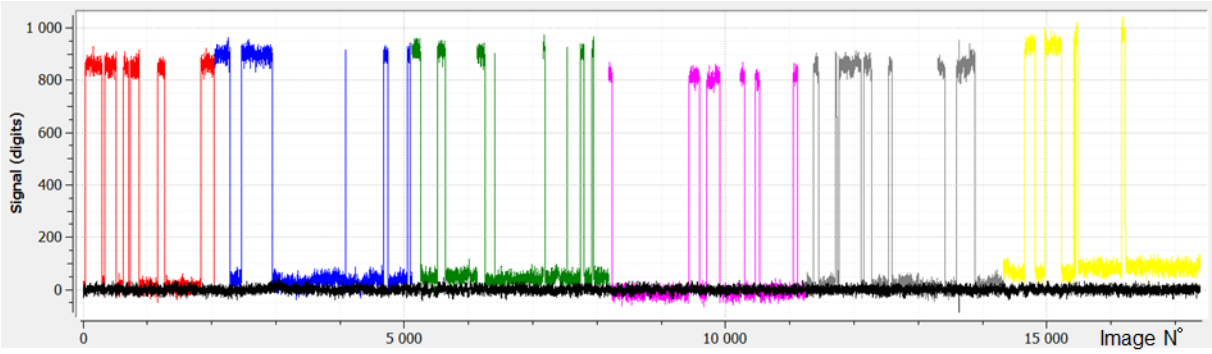

Figure 11 – Signal as a function of image number for a pixel exhibiting a 2-level RTS noise (pixel n°5409). Measurements come from the concatenation of 17 cubes of 1024 images. The color of the curve changes each time a new cooling cycle is realized. Black curve: neighboring pixel with no RTS noise.

Finally, we tried to highlight a possible link between the RTS pixels identified by these last measurements and the residual fixed pattern noise studied in the previous paragraph. It turns out that among the 10 RTS pixels identified, 7 were already counted in the 49 defective pixels. If the remaining 3 pixels are removed, bringing the number of defective pixels from 49 to 52, the RFPN/TN ratio is the same. This underlines that the criteria usually used to rule out defective pixels may miss some RTS pixels.

Conclusion

In this paper, we described our experimental protocol to evaluate the stability over time of a FPA and to count up / classify pixels with random telegraph signal noise. We presented the results obtained for a T2SL MWIR 320x256 pixels IDDCA provided by IRnova. The stability over time is excellent over seven weeks. We stressed out the importance of the criteria used to rule out defective pixels. The RFPN/TN plateau can thus be decreased from 1.1 (with reference defective pixels detection and basic two-point correction (TPC)) to 0.83 (with advanced defective pixel detection and basic TPC). If the operational application allows the use of a shutter to update one of the image cubes used for the TPC, this plateau can even be decreased to 0.6, and the periode of validity of the gain and offset coefficients extended to 6 months.

Our measurements also allowed us to count up and classify pixels exhibiting a random telegraph signal (RTS) noise. The total number of RTS pixels is 10, for a 5 minutes cumulative acquisition. Four pixels jump between 2 levels, two of them exhibit spikes while the behaviour of the four remaining pixels is difficult to analyse, thus pointing out the need to realise new measurements, on a longer time scale.

References

[1] A.K. Sood, J.W. Zeller, R.E. Welser, Y.R. Puri, N.K. Dhar, P.S. Wijewarnasuriya, S. Krishna, Design and Development of Two-Dimensional Strained Layer Superlattice (SLS) Detector Arrays for

IR Applications, Two-dimensional Materials for Photodetector Pramoda Kumar Nayak, IntechOpen (2018).
[2] A. Rogalski, M. Kopytko, P. Martyniuk, InAs/GaSb type-II superlattice infrared detectors: three decades of development, Proc. SPIE 10177 (2017) 1017715.
[3] R. Chevallier, A. Haddadi, M. Razeghi, Dark current reduction in microjunction-based compound electron barrier type-II InAs/InAs1-xSbx superlattice-based long-wavelength infrared photodetectors, Proc. SPIE 10540 (2018) 1054007.
[4] D.Z. Ting, A. Soibel, A. Khoshakhlagh, L. Höglund, S.A. Keo, S.B. Rafol, C.J. Hill, A.M. Fisher, E.M. Luong, J. Nguyen, J.K. Liu, J.M. Mumolo, B.J. Pepper, S.D. Gunapala, Antimonide type-II superlattice barrier infrared detectors, Proc. SPIE 10177 (2017) 101770N.
[5] P.C. Klipstein, E. Avnon, Y. Benny, A. Fraenkel, A. Glozman, E. Hojman, E. Ilan, E. Kahanov, O. Klin, L. Krasovitski, L. Langof, I. Lukomsky, M. Nitzani, L. Shkedy, I. Shtrichman, N. Snapi, R. Talmor, A. Tuito, S. Vaserman, and E. Weiss, Long Wave Infrared Type II Superlattice Focal Plane Array Detector, Defence Science Journal 67 (2017) 135.
[6] L. Höglund, C. Asplund, R. Marcks von Würtemberg, H. Kataria, A. Gamfeldt, S. Smuk, H. Martijn, E. Costard, Manufacturability of type-II InAs/GaSb superlattice detectors for infrared imaging, Infrared Physics & Technology 84 (2017) 28.
[7] Q. Durlin, J.P. Perez, R. Rossignol, J.B. Rodriguez, L. Cerutti, B. Delacourt, J. Rothman, C. Cervera, P. Christol, InAs/InAsSb superlattice structure tailored for detection of the full midwave infrared spectral domain, Proc. SPIE 10111 (2017) 1011112.
[8] V. Daumer, V. Gramich, R. Müller, J. Schmidt, F. Rutz, T. Stadelmann, A. Wörl, R. Rehm, Photodetector development at Fraunhofer IAF: From LWIR to SWIR operating from cryogenic close to room temperature, Proc. SPIE 10177 (2017) 1017711.
[9] A. Kazemi, S. Myers, Z.Taghipour, S. Mathews, T. Schuler-Sandy, S. Lee, V. M. Cowan, E. Garduno, E. Steenbergen, C. Morath, G. Ariyawansa, J. Scheihing, S. Krishna, Mid-wavelength infrared unipolar nBp superlattice photodetector, Infrared Physics & Technology 88 (2018) 114.
[10] B. Tan, C. Zhang, W. Zhou, X. Yang, G. Wang, Y. Li, Y. Ding, Z. Zhang, H. Lei, W. Liu, Y. Du, L. Zhang, B. Liu, L. Wang, L. Huang, The 640 × 512 LWIR type-II superlattice detectors operating at 110 K, Infrared Physics & Technology 89 (2018) 168.
[11] J. Nghiem, J. Jaeck, J. Primot, C. Coudrain, S. Derelle, E. Huard, M. Caes, S. Bernhardt, R. Haidar, P. Christol, I. Ribet-Mohamed, MTF measurements of a type-II superlattice infrared focal plane array sealed in a cryocooler, Opt. Express 26 (2018) 11034-11045.
[12] J. Nghiem, J. Jaeck, E. Giard, M. Caes, J.B. Rodriguez, P. Christol, I. Ribet-Mohamed, MTF and FPN measurements to evaluate midwave infrared T2SL focal plane arrays, Proc. SPIE 10111 (2017) 101111D.
[13] D. L. Perry, E.L. Dereniak, Linear theory of nonuniformity correction in infrared staring sensors, Optical Engineering 32 (1993) 1854.
[14] J.M. Mooney, F.D. Sheppard, W.S. Ewing, J.E. Ewing, J. Silverman,Responsivity nonuniformity limited performance of infrared staring cameras, Optical Engineering 28 (1989) 281151.
[15] J.M. Mooney, F.D. Shepherd, Characterizing IR FPA nonuniformity and IR camera spatial noise, Infrared physics & technology 37 (1996) 595.
[16] A.I. D'Souza, M.G. Stapelbroek, E.W. Robinson, C. Yoneyama, H.A. Mills, M. Kinch, H.D. Shih, Noise attributes of LWIR HDVIP HgCdTe detectors, Journal of Electronic Materials, 37 (2008) 1318
[17] A. Brunner, L. Rubaldo, V. Destefanis, F. Chabuel, A. Kerlain, D. Bauza, N.Baier, Improvement of RTS noise in HgCdTe MWIR detectors, Journal of electronic materials 43 (2014) 3060.
[18] D. Pogány, G. Guillot, Random telegraph signal noise instabilities in lattice-mismatched InGaAs/InP photodiodes, Microelectronics Reliability 39 (1999) 341.